The Astrophysical Journal Supplement Series, 234:38 (9pp), 2018 February https://doi.org/10.3847/1538-4365/aaa07e

Spitzer Observations of the North Ecliptic Pole

H. Nayyeri[1], N. Ghotbi[1], A. Cooray[1], J. Bock[2,3], D. L. Clements[4], M. Im[5], M. G. Kim[5,6], P. Korngut[2,3], A. Lanz[3], H. M. Lee[5], D. H. Lee[6,7], M. Malkan[8], H. Matsuhara[9], T. Matsumoto[10], S. Matsuura[9,10], U. W. Nam[6], C. Pearson[11,12,13], S. Serjeant[12], J. Smidt[14], K. Tsumura[15], T. Wada[9], and M. Zemcov[2,16]
[1] Department of Physics and Astronomy, University of California Irvine, Irvine, CA 92697, USA
[2] Jet Propulsion Laboratory (JPL), National Aeronautics and Space Administration (NASA), Pasadena, CA 91109, USA
[3] Department of Physics, Mathematics and Astronomy, California Institute of Technology, Pasadena, CA 91125, USA
[4] Astrophysics Group, Imperial College, Blackett Laboratory, Prince Consort Road, London SW7 2AZ, UK
[5] Department of Physics and Astronomy, Seoul National University, Seoul 151-742, People's Republic of Korea
[6] Korea Astronomy and Space science Institute, Daejeon 34055, People's Republic of Korea
[7] University of Science and Technology, Daejeon 34143, People's Republic of Korea
[8] Department of Physics and Astronomy, University of California, Los Angeles, CA 90095-1547, USA
[9] Department of Space Astronomy and Astrophysics, the Institute of Space and Astronautical Science, Japan Aerospace Exploration Agency, Sagamihara, Kanagawa 252-5210, Japan
[10] School of Science and Technology, Kwansei Gakuin University, Sanda, Hyogo 669-1337, Japan
[11] RAL Space, Rutherford Appleton Laboratory, Chilton, Didcot, Oxfordshire OX11 0QX, UK
[12] School of Physical Sciences, The Open University, Milton Keynes, MK7 6AA, UK
[13] Oxford Astrophysics, Denys Wilkinson Building, University of Oxford, Keble Road, Oxford OX1 3RH, UK
[14] Theoretical Division, Los Alamos National Laboratory, Los Alamos, NM 87545, USA
[15] Frontier Research Institute for Interdisciplinary Science, Tohoku University, Sendai, 980-8578, Japan
[16] Center for Detectors, School of Physics and Astronomy, Rochester Institute of Technology, Rochester NY 14623, USA
Received 2017 September 3; revised 2017 November 8; accepted 2017 November 19; published 2018 February 8

Abstract

We present a photometric catalog for *Spitzer Space Telescope* warm mission observations of the North Ecliptic Pole (NEP; centered at R.A. = $18^h00^m00^s$, decl. = $66^d33^m38^s.552$). The observations are conducted with IRAC in the 3.6 and 4.5 μm bands over an area of 7.04 deg^2, reaching 1σ depths of 1.29 μJy and 0.79 μJy in the 3.6 μm and 4.5 μm bands, respectively. The photometric catalog contains 380,858 sources with 3.6 and 4.5 μm band photometry over the full-depth NEP mosaic. Point-source completeness simulations show that the catalog is 80% complete down to 19.7 AB. The accompanying catalog can be used for constraining the physical properties of extragalactic objects, studying the AGN population, measuring the infrared colors of stellar objects, and studying the extragalactic infrared background light.

Key words: infrared: galaxies – infrared: stars – surveys

Supporting material: machine-readable table

1. Introduction

A statistical understanding of galaxy properties could be achieved by measuring the number counts of observed sources as a function of brightness in wide-area surveys (Jones et al. 1991; Pozzetti et al. 1998; Yasuda et al. 2001; Hatsukade et al. 2011; Valiante et al. 2016; Geach et al. 2017; Hemmati et al. 2017). This has been utilized successfully in the optical and near-infrared bands to study galaxy mass assembly and star formation activity originating from stellar emission (e.g., Gardner et al. 1993; Fontana et al. 2014). Infrared observations of extragalactic sources have been made possible by the first generations of upper-atmosphere probes and space missions (Harwit et al. 1966; Neugebauer & Leighton 1969; Neugebauer et al. 1984; Kessler et al. 1996), providing the first studies of non-stellar emission (Saunders et al. 1990; Genzel et al. 1998). In particular, all-sky observations by the *Infrared Astronomical Satellite* (Neugebauer et al. 1984) and *Wide-Field Infrared Survey Explorer* (*WISE*; Wright et al. 2010) provided the first dust maps (Schlegel et al. 1998) and paved the way for detailed studies of populations of infrared-bright galaxies (Soifer et al. 1984; Genzel et al. 1998; Calzetti et al. 2000; Eisenhardt et al. 2012; Wu et al. 2012; Bridge et al. 2013).

The *Spitzer Space Telescope* (Werner et al. 2004) revolutionized studies of galaxy evolution by making crucial observations in the infrared that revealed dust and stellar components in astronomical objects (Pérez-González et al. 2005; Draine & Li 2007; Magnelli et al. 2011). *Spitzer* deep and wide-field infrared observations over the past decade have produced a unique data set (Dickinson et al. 2003; Lonsdale et al. 2003; Sanders et al. 2007; Ashby et al. 2009, 2013b, 2015) that has been used to study galaxy formation and evolution across a wide range of redshift and physical properties (Lacy et al. 2004; Le Floc'h et al. 2005; Brandl et al. 2006; Papovich et al. 2006).

In this work, we present catalogs of stellar and galactic objects identified from *Spitzer* Infrared Array Camera (IRAC; Fazio et al. 2004) observations of the North Ecliptic Pole (NEP). The NEP (centered at R.A. = $18^h00^m00^s$, decl. = $66^d33^m38^s.552$) is the natural extragalactic deep field and has one of the deepest observations by several space observatories, including *Planck* and *AKARI* (Serjeant et al. 2012). Furthermore, it has extensive observations from the X-ray to the millimeter (Kollgaard et al. 1994; Gioia et al. 2003; Lee et al. 2007; Jeon et al. 2010, 2014; Krumpe et al. 2015), with additional observations by *WISE* (Jarrett et al. 2011). The field was specifically chosen to match the observations by the Cosmic Infrared Background Experiment (CIBER; Bock et al. 2013; Zemcov et al. 2014 as per msp) to study the extragalactic background light fluctuation (Cooray et al. 2004, 2012a; Matsumoto et al. 2005; Zemcov et al. 2014; Matsuura

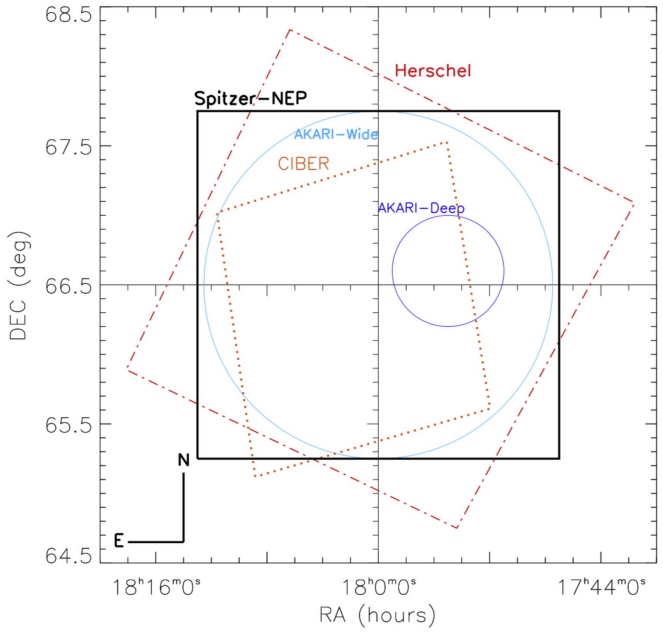

Figure 1. The areal coverage of the *Spitzer* NEP (centered at R.A. = $18^h00^m00^s$, decl. = $66^d33^m38^s.552$) compared to that of *AKARI* (Murakami et al. 2007) in the deep (Matsuhara et al. 2006; Murata et al. 2013) and wide (Lee et al. 2009) fields, CIBER (Bock et al. 2013; Zemcov et al. 2014), and *Herschel* (Pearson et al. 2017). The *Spitzer* observations were chosen to maximize the sky coverage by all these surveys, providing a complete census of the infrared SEDs of galaxies.

et al. 2017). Figure 1 shows the sky coverage of the *Spitzer* NEP observations compared to the other infrared missions of the NEP (Murakami et al. 2007; Matsuhara et al. 2006; Lee et al. 2009; Pilbratt et al. 2010; Bock et al. 2013; Murata et al. 2013). The *Spitzer* observations were designed to maximize overlap with those of *AKARI* (Murakami et al. 2007) in the deep (Matsuhara et al. 2006; Murata et al. 2013) and wide (Lee et al. 2009) fields and observations by *Herschel* (Pearson et al. 2017).

The *Spitzer*/IRAC data set is complementary to the already existing optical/near-infrared (Jeon et al. 2010, 2014) data and could be used in combination with those pre-existing data to constrain the stellar mass function of galaxies in the NEP. The *Spitzer* infrared observations in the NEP could additionally be utilized (in conjunction with the already existing X-ray observations; Krumpe et al. 2015) to identify AGNs (Stern et al. 2005). The NEP imaging data are particularly important for studies of diffuse light background fluctuations arising from individually undetected sources directly probing early star formation (Cooray et al. 2004, 2012a; Zemcov et al. 2014).

The paper is organized as follows. In Section 2 we present the imaging data and compilation for the *Spitzer* NEP field. Section 3 provides details on our source catalog and photometry estimation. We discuss our data analysis results in Section 4 and summarize our findings in Section 5. Throughout this paper we assume a standard cosmology with $H_0 = 70\,\mathrm{km\,s^{-1}\,Mpc^{-1}}$, $\Omega_m = 0.3$, and $\Omega_\Lambda = 0.7$. All magnitudes are in the AB system where $m_{\rm AB} = 23.9–2.5 \times \log(f_\nu/1\ \mu\mathrm{Jy})$ (Oke & Gunn 1983).

2. Data

The NEP, centered at R.A. = $18^h00^m00^s$, decl. = $66^d33^m38^s.552$, was observed with *Spitzer*/IRAC in Cycle 10 (Program ID: 10147; PI: J. Bock). The observations were carried out over three epochs in both the 3.6 and 4.5 μm bands (Table 1). The first two epochs were separated by ∼10 weeks and epoch three was observed ∼8 weeks after epoch two. The observations in different epochs enable study of the zodiacal light contamination, which changes throughout the year, for background fluctuations (Cooray et al. 2012a).

Three epochs were considered sufficient for mapping the *Spitzer* NEP, based on previous observations of the *Spitzer* Deep Wide-Field Survey (SDWFS) (Ashby et al. 2009), as this provided reliable power spectra measurements for studying the intrahalo light (IHL) and extragalactic background light (EBL; Cooray et al. 2012b; Zemcov et al. 2014), combined with existing CIBER and *AKARI* data in the field. The mapping strategy involved observations that were offset by one-third of the IRAC field of view between successive passes through each group (where we split the field into sixteen groups) and were dithered on small scales to maximize the inter-pixel correlation to facilitate self-calibrations. Furthermore, to ensure that asteroids are reliably identified, each group is observed in three passes of 30 s each. The time required to obtain a single 30 s pass on a group ensures gaps of at least 2 hr between observations of each sky position. For typical asteroid motions of 25 arcsec hr^{-1}, asteroids will move 1 arcmin between maps. Since this is much smaller than a typical map width, three map observations will reliably track asteroid motions. Note that there are very unlikely to be any main belt asteroids (with a 25 arcsec hr^{-1} motion) in the Ecliptic Cap, with most being near the Ecliptic Plane. Some near-Earth asteroids may be present, but these typically have much faster motions (∼several arcmin/hr) and are easily identifiable.

Basic calibrated data (BCD) and associated files were directly downloaded from the *Spitzer* Science Center after acquisition. This corresponds to 3936 tiles in each epoch in each of the bands (except epoch 2, which observed 3854 tiles in 3.6 μm; see Table 1) with 23.6 s and 26.8 s exposures per tile at 3.6 μm and 4.5 μm, respectively. This resulted in a continuous *Spitzer* map of the NEP field covering an area of 7.04 deg^2 corresponding to a total integration time of ∼165 hr. Figure 2 shows the NEP area coverage and depth compared to other *Spitzer* surveys.

We used MOPEX[17] version 18.5.0 (Makovoz et al. 2006) on the corrected-basic calibrated data (cBCDs) released by the *Spitzer* Science Center to construct the mosaics. We generated combined mosaics for each epoch and a combined mosaic of all three epochs with MOPEX for the 3.6 and 4.5 μm observations. Figure 3 shows the combined three-epoch mosaics in the 3.6 and 4.5 μm bands. In summary, MOPEX takes the data frames along with the associated uncertainty frames and constructs a Fiducial Image Frame (FIF) from the boundaries of the data frame onto which input observations will be projected. It then runs a background matching routine on overlapping frames and performs an image interpolation that maps the individual frames onto the generated FIF, after which a co-added mosaic image is generated. During the process MOPEX also performs an outlier rejection routine to identify outlier pixels (such as cosmic rays) and generates a bad pixel mask that is used in the construction of the mosaic. Each generated science map is also accompanied by the corresponding uncertainty and exposure maps calculated by MOPEX. We refer the reader to the MOPEX

[17] http://irsa.ipac.caltech.edu/data/SPITZER/docs/dataanalysistools/tools/mopex/

Table 1
Observations Summary[a]

Epoch	Observation Dates	No. BCDs 3.6 μm/4.5 μm	Exposure Time[b] 3.6 μm/4.5 μm	Exposure Time per pixel[c] 3.6 μm/4.5 μm
			(hr)	(s)
1	2014 May 06–09	3936/3936	25.8/29.3	106/120
2	2014 Jul 18–24	3854/3936	25.3/29.3	104/119
3	2014 Sep 08–14	3936/3936	25.8/29.3	107/121
Total	…	11808/11726	76.9/87.9	282/331[d]

Notes.
[a] Cycle 10 program *Spitzer*/IRAC observations (PID: 10147).
[b] Total exposure time of each mosaic.
[c] The average exposure time per pixel in each mosaic.
[d] Measured as the average value from the combined three-epoch mosaic exposure maps.

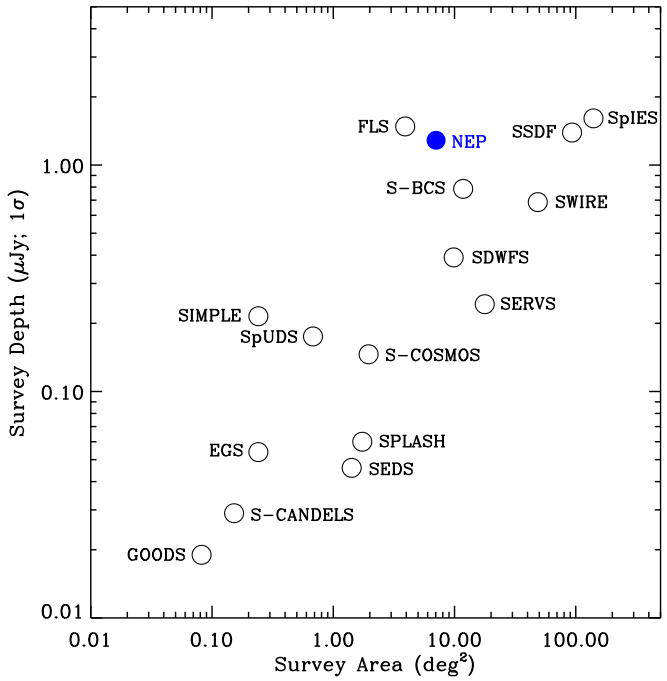

Figure 2. Observation depth and sky coverage of the NEP (at the 3.6 μm) compared to other *Spitzer* surveys. These include the Great Observatories Origins Deep Survey (GOODS; Dickinson et al. 2003; Giavalisco et al. 2004), the *Spitzer*-Cosmic Assembly Near-infrared Deep Extragalactic Legacy Survey (S-CANDELS; Ashby et al. 2015), the Extended Groth Strip (EGS; Davis et al. 2007), the *Spitzer* Extended Deep Survey (SEDS; Ashby et al. 2013b), the *Spitzer* Large Area Survey with Hyper-Suprime-Cam (SPLASH; Capak et al. 2013), S-COSMOS (Sanders et al. 2007), the *Spitzer* Public Legacy Survey of UKIDSS Ultra-deep Survey (SpUDS; Caputi et al. 2011), the *Spitzer* IRAC/MUSYC Public Legacy in E-CDFS (SIMPLE; Damen et al. 2011), the *Spitzer* Deep Wide-Field Survey (SDWFS; Ashby et al. 2009), the *Spitzer* Wide-area Infrared Extragalactic Survey (SWIRE; Lonsdale et al. 2003), the *Spitzer* Blanco Cluster Survey (S-BCS), the First Look Survey (FLS; Lacy et al. 2005), the *Spitzer* Extragalactic Representative Volume Survey (SERVS; Mauduit et al. 2012), the *Spitzer*-IRAC Equatorial Survey (SpIES) , and the *Spitzer* South Pole Telescope Deep Field (SSDF; Ashby et al. 2013a). The NEP covers an area of 7.04 deg^2 reaching a 1σ depth of 1.29 μJy (measured over an aperture of 4″).

manual for further details.[18] Figure 4 shows the MOPEX-generated coverage map of the NEP for the full-depth mosaics in the 3.6 and 4.5 μm bands. We see that the NEP observations have very uniform depth across the field in both bands. Figure 5 shows the area coverage of the 3.6 μm map given a minimum exposure time for a single epoch and the full-depth mosaics. We see that more than 89% of the field (with area ~6.26 deg^2) is covered with an exposure time of at least 100 s in the full-depth mosaic, whereas only 45% (with area ~3.17 deg^2) is covered to similar depths in a single epoch. The individual 3.6 μm epochs have 1σ depths of 2.11 μJy, 2.13 μJy, and 2.22 μJy, respectively in the three epochs and a depth of 1.29 μJy over the combined full-depth mosaic. The combined full-depth mosaic in the 4.5 μm band has a 1σ depth of 0.79 μJy (measured over an aperture of 4″ with aperture corrections applied; see Section 3.2). Table 1 summarizes the *Spitzer* NEP observations.

[18] http://irsa.ipac.caltech.edu/data/SPITZER/docs/dataanalysistools/tools/mopex/mopexusersguide/

3. Source Catalogs

3.1. Source Identification and Photometry

We used SExtractor (Bertin & Arnouts 1996) for source identification and photometry. SExtractor is run in dual mode on the combined three-epoch mosaics on the 3.6 μm and 4.5 μm individually, as the detection bands with photometry are extracted in both. The two catalogs are then merged to form the final NEP catalog. With this approach, we make sure to include 3.6 μm faint sources that are detected in the 4.5 μm and would have been missed by the former selection alone. The MOPEX-generated mosaics are in units of [MJy Sr^{-1}], which we convert to [μJy pixel^{-1}] using the map pixel scale of 1.″2 before measuring the photometry. We used a minimum detection area of 3 pixels with a detection threshold of 2σ for source identification. This is chosen to maximize the recovered sources while minimizing spurious source identification. We identify 380,858 sources over the 7.04 deg^2 area of the *Spitzer* NEP map with our detection criteria. We measure source photometry in AB magnitudes given the pixel flux units in micro-Jansky and report this in a Kron radius (the MAG_AUTO), which is photometry over an ellipse with its size and orientation determined from the second moment of light distribution above the isophotal threshold, and also over two apertures (with 4″ and 6″ diameter). We further report the SExtractor measured stellarity parameter for each object, which we use later (see Section 4.4) to validate the color of stars in the field. Figure 6 shows the area-normalized distribution of the source photometry in the full NEP of the combined three epochs.

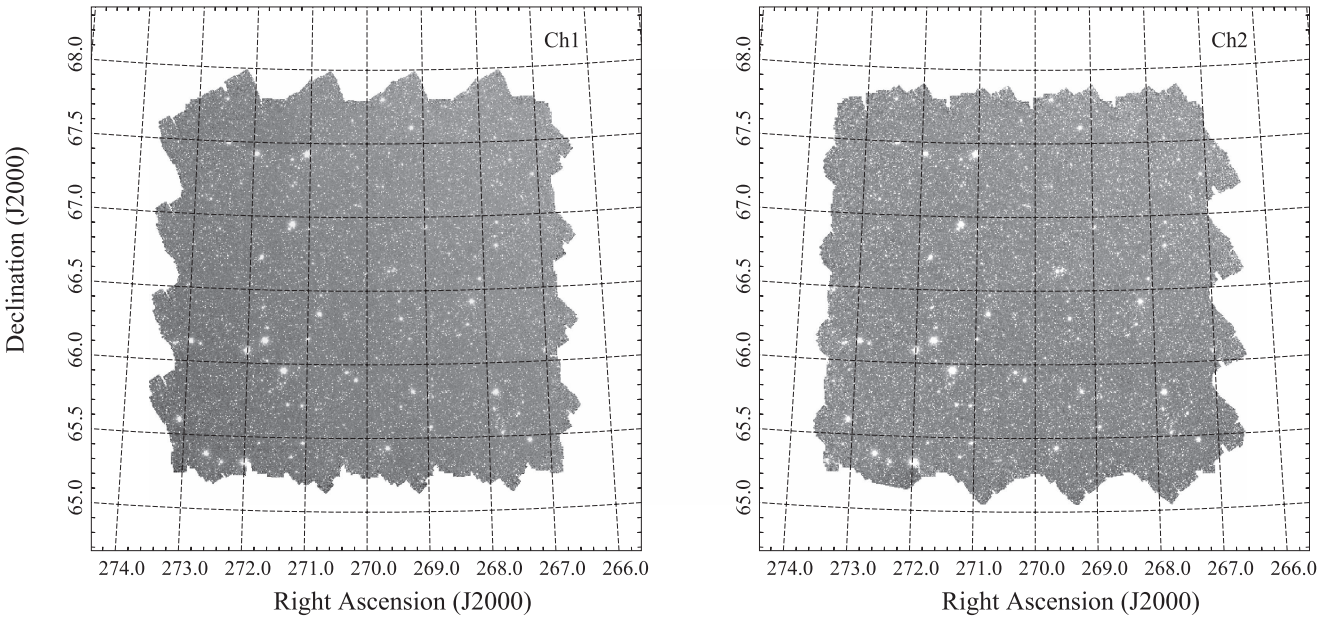

Figure 3. Combined three-epoch *Spitzer* maps of the NEP in the 3.6 μm (left) and the 4.5 μm band (right) as part of Cycle 10 observations with a total exposure time of ~165 hr during the warm mission, over an area ~7.04 deg^2.

3.2. Aperture Corrections

We perform aperture photometry over two circular apertures at fixed 4″ and 6″ diameters in addition to the SExtractor measured MAG_AUTO discussed above. The fixed apertures often underpredict the flux of objects. We corrected the aperture photometry measurements in the 3.6 and 4.5 μm bands for the effect of fixed apertures (at 4″ and 6″) used in their measurements. For this, we used the curve of growth of five isolated stars in the field, using ever-growing circular apertures (with 4″–10″ diameter) to measure the source flux. The aperture correction is measured as the mean of the correction from the curve of growth of the selected stars. Table 2 summarizes the aperture corrections (in AB magnitudes) for both observed IRAC bands. These agree with the reported numbers by Ashby et al. (2009) for SDWFS and also corrections reported by the IRAC Instrument Handbook.

3.3. Astrometry

We validate the astrometry of the *Spitzer* NEP catalog generated by SExtractor against the publicly available USNO CCD Astrograph Catalog's (UCAC; Zacharias et al. 2013) fourth version.[19] We use a 2″ radius to cross-match the NEP catalog with that of UCAC. We further limit the astrometry analysis to sources with a minimum signal-to-noise ratio of 20 in the NEP 3.6 μm band. This generates a catalog of 8729 sources over the full NEP area. Figure 7 shows the distribution of the difference in R.A. and decl. between the NEP catalog and the UCAC. The distribution of the difference in decl. is consistent with being centered on zero with a deviation of 0.″04, whereas the R.A. difference shows a mean offset of 0.″25. These distributions have standard deviations of 0.″51 and 0.″24 in the R.A. and decl., respectively, smaller than the IRAC spatial resolution measured from the PSF FWHM (~1.″78). We note here that the offset is also smaller than the pixel scale of our *Spitzer*/IRAC mosaics at 1.″2 and that we did not apply this to the final photometric catalog. The final photometric catalog will be available through the IRSA website[20] and as a machine readable table with this publication. Table 3 summarizes the entries in the published catalog.

4. Analysis

4.1. Number Counts

The *Spitzer* NEP 3.6 μm selected catalog has 380,858 sources over an area of 7.04 deg^2. Figure 6 shows the NEP area-normalized source number counts, along with the source counts from SDWFS (Ashby et al. 2009) in the 3.6 and 4.5 μm bands. The variations in the number count distributions are associated with the larger number of stars and shallower depths (see Figure 2) at the bright and faint ends, respectively, in the NEP, compared to that of SDWFS. Table 4 summarizes the source counts of the photometric catalog in designated magnitude bins, along with the associated Poisson uncertainties.

4.2. Completeness Estimates

To get an estimate of the NEP survey catalog depth, we performed a point-source completeness estimate on the combined three-epoch full-depth in the 3.6 μm band. For this we generated a large number of point sources of varying brightness (with 1000 sources in each 0.05 bin of magnitude), given the IRAC PSF FWHM (at 1.″78). We then randomly distributed these sources across the 3.6 μm mosaic while avoiding the mosaic edges and existing objects in the field using the segmentation map generated by SExtractor for the main photometric catalog. We used the original SExtractor detection criteria to identify sources in the new co-added map of real and simulated objects. We cross-matched the generated

[19] http://www.usno.navy.mil/USNO/astrometry/optical-IR-prod/ucac

[20] http://irsa.ipac.caltech.edu/Missions/spitzer.html

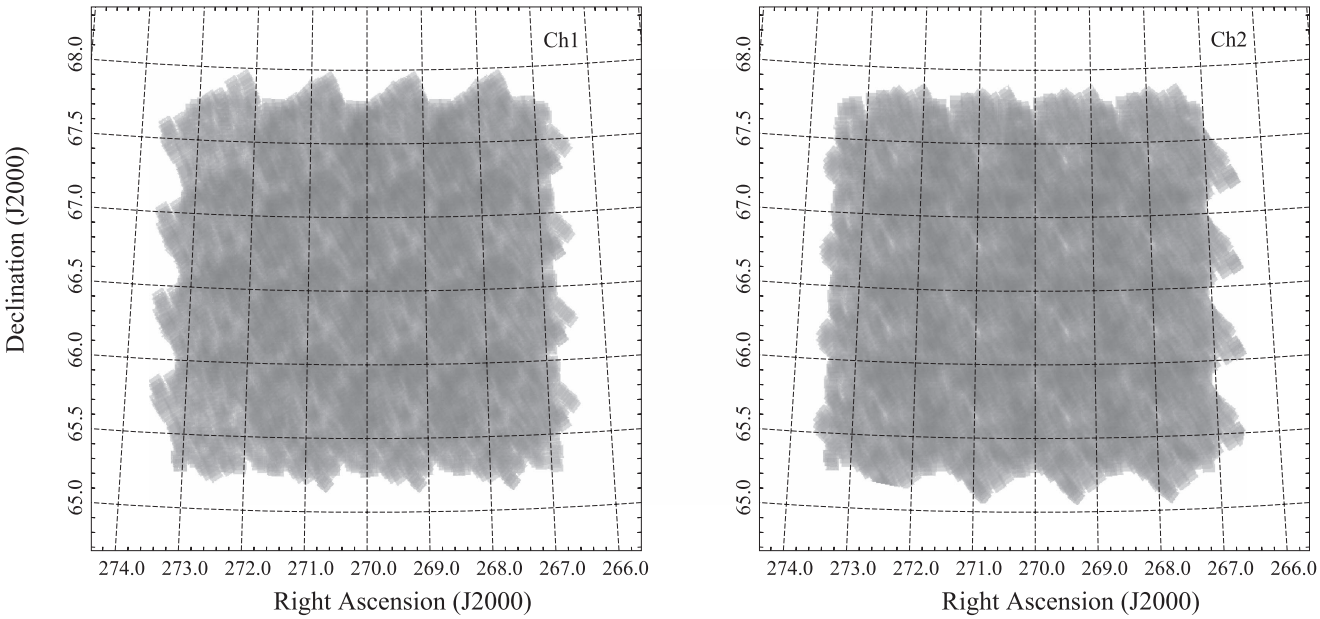

Figure 4. Combined three-epoch *Spitzer* 3.6 μm (left) and 4.5 μm (right) coverage maps demonstrating the depth uniformity across the field. This consists of a total of 11808 and 11726 individual tiles in the 3.6 μm and 4.5 μm bands, respectively, over three epochs.

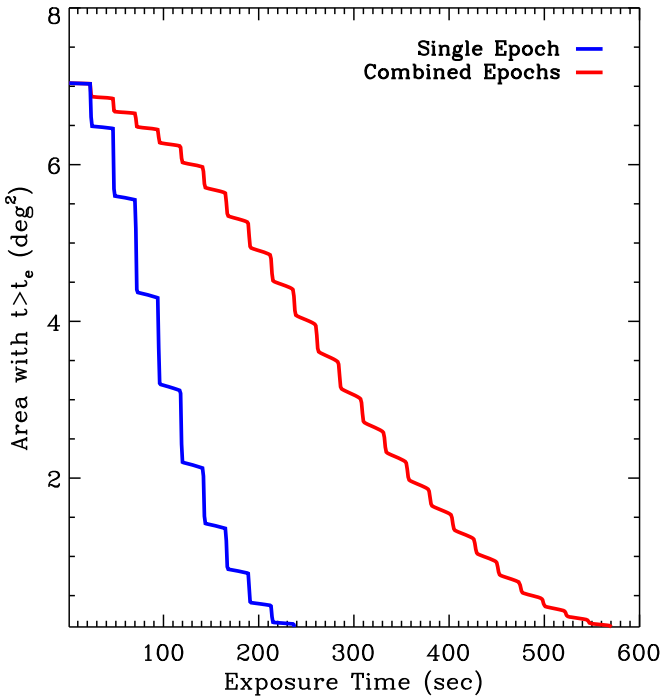

Figure 5. Area coverage of the *Spitzer* 3.6 μm NEP map as a function of total exposure time for the combined three epochs (in red) and a single epoch (in blue). More than 89% of the field is covered with an exposure time of at least 100 s in the combined mosaic where that number is 45% for the single epoch observations. Table 1 summarizes the exposure time in each epoch.

catalog with the known simulated positions of the injected sources, which yields a recovery fraction of the point sources. Figure 8 shows the recovered fraction of the simulated point sources as a function of the source brightness. The catalog has a point-source completeness estimate of 80% for objects with 19.71 (AB mag) in the 3.6 μm and drops rapidly for faint sources.

4.3. Photometric Validation Check

To check the robustness of the *Spitzer* measured photometry, we compared our IRAC measured photometry with that of *WISE* (Wright et al. 2010). For this, we used the AllWISE catalog (Cutri 2013) to extract the *WISE* photometry in the W1 and W2 bands (at 3.4 μm and 4.6 μm, respectively). We used the conversion factors provided in Table 1 of Jarrett et al. (2011) to convert the *WISE* measured Vega magnitudes in the W1 and W2 bands to AB magnitudes for comparison. Figure 9 shows the comparison of *Spitzer* measured magnitudes in the 3.6 μm and 4.5 μm bands to that of *WISE* W1 and W2 observations in the NEP. The *Spitzer* measured photometry is consistent with that of *WISE,* with a small scatter at bright magnitudes ($\sigma(m) = 0.03$ for 3.6 μm and $\sigma(m) = 0.01$ for 4.5 μm; computed at $m_{\rm AB} = 15$), increasing to $\sigma(m) = 0.23$ for 3.6 μm and $\sigma(m) = 0.32$ for 4.5 μm for fainter objects (measured at $m_{\rm AB} = 20$). The *Spitzer* photometry is offset from *WISE* by $\Delta m = 0.13$ and $\Delta m = 0.07$ in the 3.6 μm and 4.5 μm bands, respectively (measured from the bright end). This is associated with differences in the filter response functions and effective wavelengths probed creating a zero-point offset. We do not apply these offsets to our *Spitzer* NEP photometric catalog.

We further compared our IRAC photometry in the *Spitzer* NEP with infrared observations by the *AKARI* in the NEP. For this we used the catalog of sources in the *AKARI* deep and wide surveys of the NEP (Kim et al. 2012; Murata et al. 2013), covering areas of 0.5 deg^2 and 5.4 deg^2, respectively. Figure 9 shows a comparison of the 3.6 μm photometry to that of *AKARI*. For comparison, we take the average of the fluxes in the *AKARI* N3 and N4 filters (at 3.2 μm and 4.1 μm, respectively; Murata et al. 2013). We see from the figure that, on average, the measured IRAC 3.6 μm photometry agrees well with that of *AKARI*, specially at the bright end and for the *AKARI* deep observations. The main source of the deviation is associated with the differences in the *Spitzer* filter response

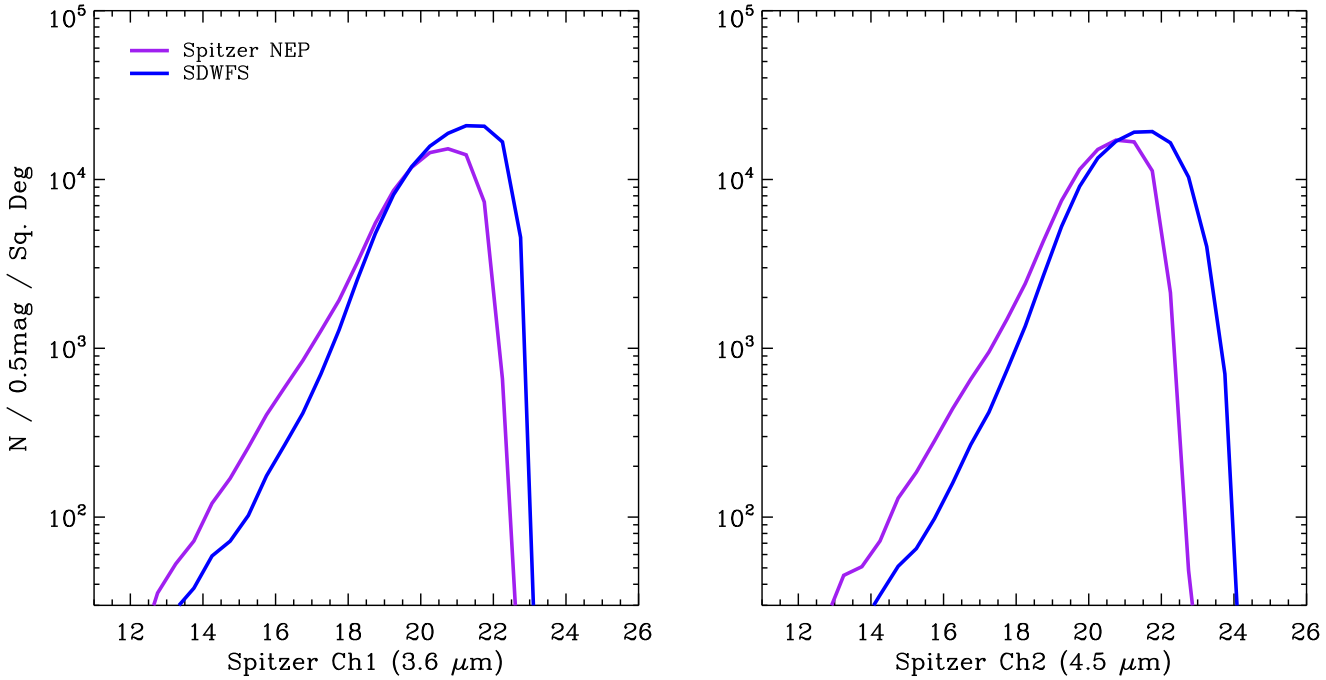

Figure 6. Left: normalized 3.6 μm number counts of sources in the *Spitzer* NEP catalog (magenta) compared to the counts in the SDWFS (blue). The SDWFS is a deeper survey (see Figure 2), which is reflected in the counts at the faint end. On the other hand, the *Spitzer* NEP shows a larger number of sources at the bright end. Right: number counts of sources in the *Spitzer* NEP 4.5 μm band, compared to those for SDWFS (Ashby et al. 2009).

Table 2
Aperture Corrections[a]

Aperture Diameter	3.6 μm band	4.5 μm band
3″	−0.65	−0.65
4″	−0.36	−0.46
5″	−0.22	−0.28
6″	−0.15	−0.19

Note.
[a] Measured from point -source curves of growth.

function and the average filter functions associated with the combined *AKARI* N3 and N4 observations.

4.4. IRAC Color

We further check the validity of the *Spitzer* measured photometry by comparing the color distribution of stars in the NEP survey to the expected infrared color derived from stellar model templates. For this we used the BaSeL stellar library (Lejeune et al. 1997, 1998; Westera et al. 2002) and computed the expected color of model templates by integrating over the stellar SEDs given the *Spitzer*/IRAC filter response functions[21] at 3.6 and 4.5 μm. Figure 10 shows the expected Ch2 [4.5 μm] − Ch1 [3.6] μm color of stellar models compared to measured colors of stars in the NEP catalog. We identified stellar sources in the NEP catalog using the stellarity parameter, CLASS_STAR, from SExtractor requiring CLASS_STAR > 0.99. This gives 2107 stellar objects for the NEP catalog. The IRAC color distribution of stars in the NEP catalog is consistent with stellar model predictions with mean (4.5–3.6 μm) values of 0.47 and 0.50 for the observed color of stars from NEP catalog and measured color from template stellar models, respectively. The scatter in the NEP IRAC colors is associated with the photometric uncertainties in individual flux measurements.

[21] http://irsa.ipac.caltech.edu/data/SPITZER/docs/irac/calibrationfiles/spectralresponse/

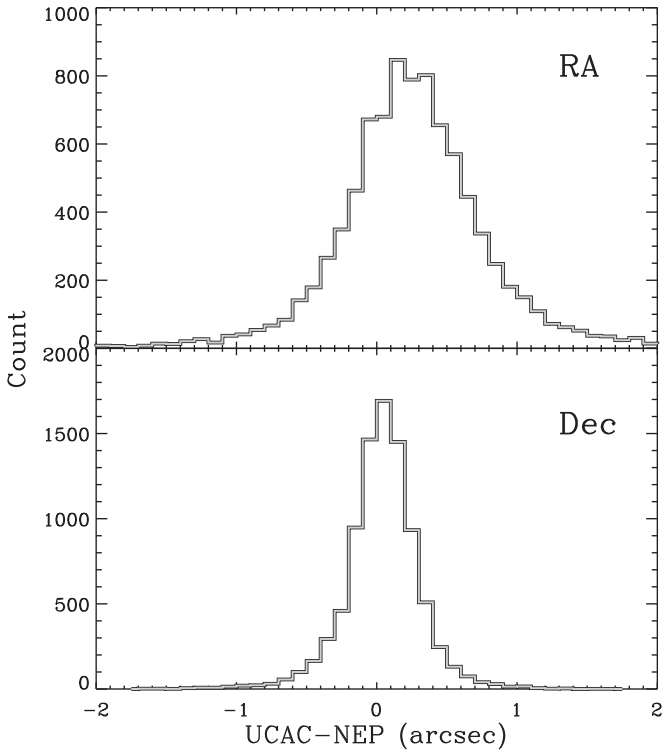

Figure 7. Distribution of the difference in R.A. (top) and decl. (bottom) of the *Spitzer* NEP catalog relative to that of the USNO CCD Astrograph Catalog (UCAC4; Zacharias et al. 2013). The NEP shows an offset of 0.″25 in the R.A. (smaller than the *Spitzer* mosaic pixel) compared to the UCAC catalog, whereas the decl. distribution is consistent with a zero offset. The distributions have standard deviations of 0.″51 and 0.″24 in the R.A. and decl., respectively, that are smaller than that of the IRAC PSF FWHM.

Table 3
The *Spitzer*/IRAC Photometric Catalog for the North Ecliptic Pole

Column	Explanation
# 1	Sequential number identifier
# 2	R.A. of Target
# 3	Decl. of Target
# 4	IRAC 3.6 μm Auto (Kron radius) Magnitude (AB)
# 5	IRAC 3.6 μm Auto Magnitude Error (AB)
# 6	IRAC 4.5 μm Auto (Kron radius) Magnitude (AB)
# 7	IRAC 4.5 μm Auto Magnitude Error (AB)
# 8	IRAC 3.6 μm 4″ diameter aperture Magnitude (AB)
# 9	IRAC 3.6 μm 4″ diameter aperture Magnitude Error (AB)
# 10	IRAC 4.5 μm 4″ diameter aperture Magnitude (AB)
# 11	IRAC 4.5 μm 4″ diameter aperture Magnitude Error (AB)
# 12	IRAC 3.6 μm 6″ diameter aperture Magnitude (AB)
# 13	IRAC 3.6 μm 6″ diameter aperture Magnitude Error (AB)
# 14	IRAC 4.5 μm 6″ diameter aperture Magnitude (AB)
# 15	IRAC 4.5 μm 6″ diameter aperture Magnitude Error (AB)
# 16	SExtractor stellarity parameter

(This table is available in its entirety in machine-readable form.)

Table 4
Spitzer/IRAC 3.6 μm Number Counts in the NEP Catalog

Spitzer/IRAC 3.6 μm[a]	N (deg^{-2} mag^{-1})	Poisson Uncertainty
14.25	121	6
14.75	170	7
15.25	259	9
15.75	404	11
16.25	586	13
16.75	845	15
17.25	1270	19
17.75	1927	23
18.25	3222	30
18.75	5522	40
19.25	8605	49
19.75	11811	58
20.25	14422	64
20.75	15205	66

Note.
[a] Bin center magnitude.

4.5. X-Ray Sources

The *Spitzer*/IRAC colors have been used to identify populations of active galaxies (Stern et al. 2005; Donley et al. 2012) where the continuum flux is expected to be dominated by a power law for AGN-dominated sources. These selections use the IRAC observations in four filters to isolate the AGN selection area on the color–color diagram. Due to a lack of longer wavelength *Spitzer* observations (at 5.8 and 8.0 μm), we instead look at the (3.6–4.5 μm) color distribution of sources in the NEP catalog. Figure 11 shows the IRAC color distribution of all the NEP sources compared to the X-ray-detected sources in the field. We used the *Chandra AKARI* NEP X-ray point-source catalog (Krumpe et al. 2015) and used a 2″ matching radius to extract the IRAC colors. This gives 354 matched sources with the X-ray catalog. We see that the X-ray sources have a redder (3.6–4.5 μm) color distribution, on average, compared to the full sample, as expected for AGN samples (Stern et al. 2005).

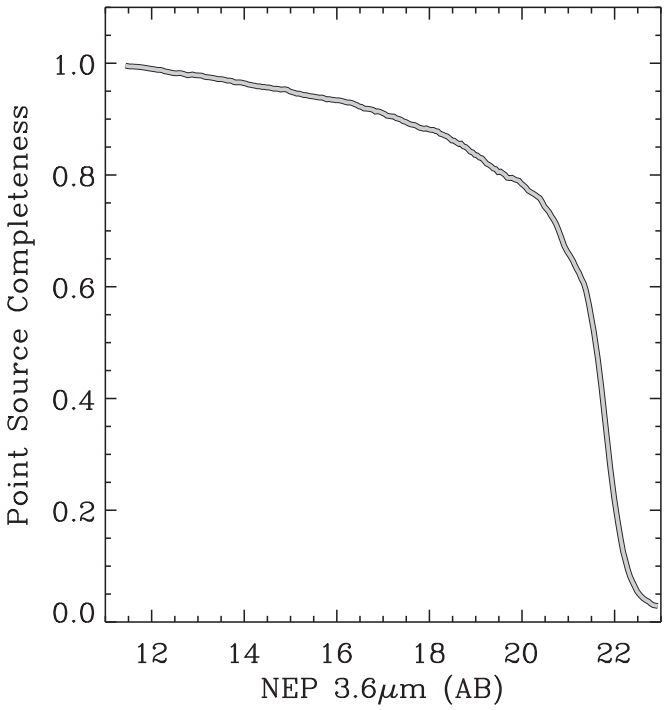

Figure 8. Simulated point-source completeness fraction at 3.6 μm as a function of source magnitude. Point sources are generated from the IRAC 3.6 μm PSF and are randomly distributed over the NEP mosaic. The recovered fraction using the original SExtractor parameters, used to generate the photometric catalog, provides the completeness.

5. Summary

Here, we presented *Spitzer*/IRAC combined mosaics and a 3.6 and 4.5 μm detected catalog of extragalactic sources in the North Ecliptic Pole (centered at R.A. $= 18^{h}00^{m}00^{s}$, decl. $= 66^{d}33^{m}38\overset{s}{.}552$). The catalog contains IRAC photometry for 380,858 sources in the 3.6 and 4.5 μm bands. Here are the main findings:

1. The combined three-epoch full-depth mosaic covers an area of 7.04 deg^2, reaching 1σ depths of 1.29 μJy and 0.79 μJy, over an aperture of 4″ in diameter, in the 3.6 μm and 4.5 μm bands, respectively.
2. The mosaics have uniform exposure across the field, with more than 89% of the field covered by an exposure time of at least 100 s.
3. The photometric catalog has astrometry offset and uncertainties consistent with the *Spitzer* PSF FWHM and pixel size.
4. The *Spitzer*/IRAC measured photometry in the NEP is consistent with earlier measurements by *WISE* and *AKARI* at similar wavelengths, with current IRAC observations being deeper than both.
5. The colors of stellar objects in the NEP agree with colors of stellar template models and also agree with expected colors of X-ray-detected sources, further validating the measured photometry.
6. The generated IRAC point-source catalogs will be available through the NASA/IPAC Infrared Science Archive.

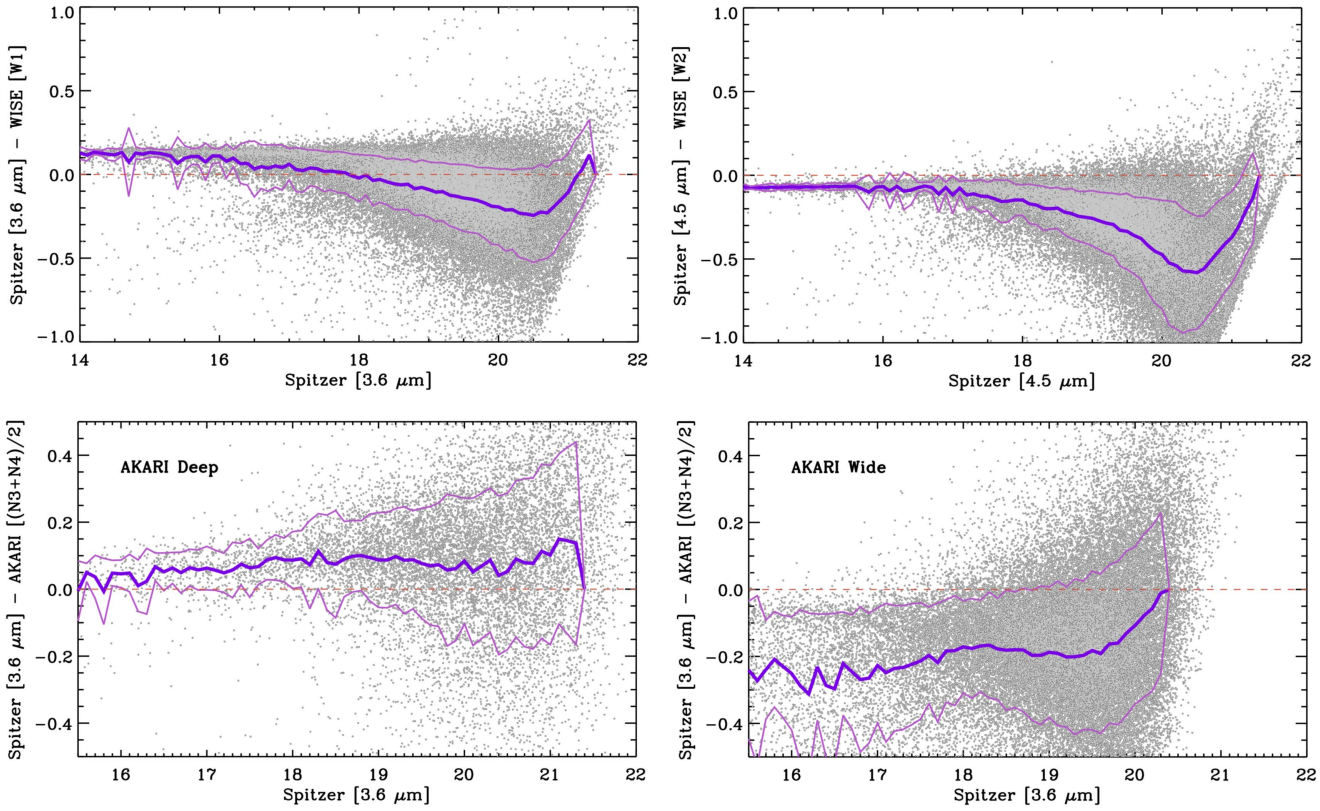

Figure 9. Top: photometric comparison of the *Spitzer* NEP to that of *WISE* (Wright et al. 2010) for the NEP 3.6 μm (left) and 4.5 μm bands. We use the AllWISE catalog (Cutri 2013) photometry measurements in the W1 (at 3.4 μm) and W2 (at 4.6 μm) bands to compare with NEP catalogs, respectively. The NEP photometry is consistent with *WISE* showing small scatter, with magnitude offsets associated with variations in the filter response function shapes between *Spitzer* and *WISE*. Bottom: photometric comparison of the IRAC 3.6 μm in the NEP to that of the *AKARI* deep (left; Murata et al. 2013) and *AKARI* wide (right; Kim et al. 2012) surveys. The *AKARI* photometry is taken from the average of the fluxes in the two *AKARI* infrared bands of N3 and N4 (at 3.2 μm and 4.1 μm, respectively).

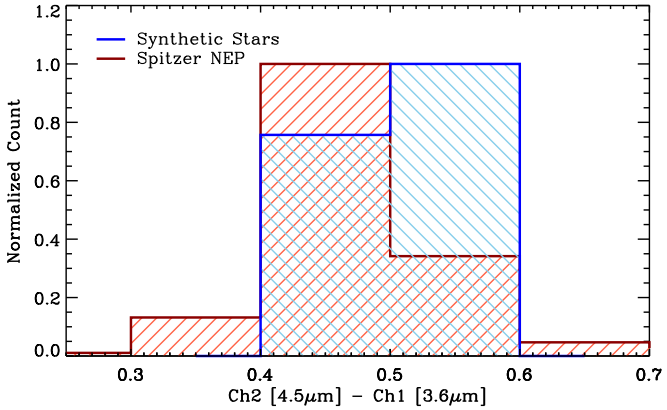

Figure 10. Observed (4.5–3.6 μm) color distributions of stars in the *Spitzer* NEP catalog (in red) compared to the color of template stellar models from the BaSeL library (Lejeune et al. 1997, 1998; Westera et al. 2002). The NEP stars are selected using the SExtractor stellarity parameter assuming CLASS_STAR > 0.9. The stellar model colors are computed using the *Spitzer* filter response functions. The observed IRAC color of stars is consistent with predictions from the BaSeL library, with mean colors of 0.54 and 0.51. The scatter in the observed IRAC color is associated with the photometric uncertainties in the NEP catalog.

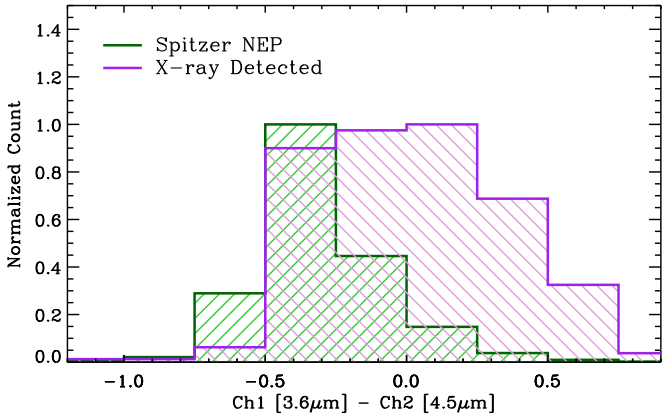

Figure 11. The observed IRAC (3.6–4.5 μm) color distribution of all *Spitzer* NEP sources (in green) compared to the X-ray detected objects (Krumpe et al. 2015; in magenta). The distribution of the IRAC colors of X-ray sources is consistent with the AGN colors reported in Stern et al. (2005).

We wish to thank the referee for reading the original manuscript and providing useful suggestions. Financial support for this work was provided by NSF through AST-1313319 for H.N. and A.C. The UCI group also acknowledges support from HST-GO-14083.002-A, HST-GO-13718.002-A, and NASA NNX16AF38G grants. M.I. acknowledge the support from the NRFK grant, No. 2017R1A3A3001362. This work was supported by NASA APRA research grants NNX07AI54G, NNG05WC18G, NNX07AG43G, NNX07AJ24G, and NNX10AE12G. This work is based on observations made with the *Spitzer Space Telescope*, which is operated by the Jet Propulsion Laboratory, California Institute of Technology under a contract with NASA. Support for this work was provided by NASA through an award issued by JPL/Caltech.

ORCID iDs

H. Nayyeri https://orcid.org/0000-0001-8242-9983
D. L. Clements https://orcid.org/0000-0002-9548-5033
M. Im https://orcid.org/0000-0002-8537-6714
M. G. Kim https://orcid.org/0000-0001-9000-9209
M. Malkan https://orcid.org/0000-0001-6919-1237
T. Matsumoto https://orcid.org/0000-0001-6066-5221
S. Matsuura https://orcid.org/0000-0002-5698-9634
C. Pearson https://orcid.org/0000-0001-6139-649X
S. Serjeant https://orcid.org/0000-0002-0517-7943
J. Smidt https://orcid.org/0000-0002-7527-3674
K. Tsumura https://orcid.org/0000-0001-7143-6520
M. Zemcov https://orcid.org/0000-0001-8253-1451

References

Ashby, M. L. N., Stanford, S. A., Brodwin, M., et al. 2013a, ApJS, 209, 22
Ashby, M. L. N., Stern, D., Brodwin, M., et al. 2009, ApJ, 701, 428
Ashby, M. L. N., Willner, S. P., Fazio, G. G., et al. 2013b, ApJ, 769, 80
Ashby, M. L. N., Willner, S. P., Fazio, G. G., et al. 2015, ApJS, 218, 33
Bertin, E., & Arnouts, S. 1996, A&AS, 117, 393
Bock, J., Sullivan, I., Arai, T., et al. 2013, ApJS, 207, 32
Brandl, B. R., Bernard-Salas, J., Spoon, H. W. W., et al. 2006, ApJ, 653, 1129
Bridge, C. R., Blain, A., Borys, C. J. K., et al. 2013, ApJ, 769, 91
Calzetti, D., Armus, L., Bohlin, R. C., et al. 2000, ApJ, 533, 682
Capak, P., Aussel, H., Bundy, K., et al. 2013, Spitzer Proposal 10042
Caputi, K. I., Cirasuolo, M., Dunlop, J. S., et al. 2011, MNRAS, 413, 162
Cooray, A., Bock, J. J., Keatin, B., Lange, A. E., & Matsumoto, T. 2004, ApJ, 606, 611
Cooray, A., Gong, Y., Smidt, J., & Santos, M. G. 2012a, ApJ, 756, 92
Cooray, A., Smidt, J., de Bernardis, F., et al. 2012b, Natur, 490, 514
Cutri, R. M., et al. 2013, yCat, 2328, 0
Damen, M., Labbé, I., van Dokkum, P. G., et al. 2011, ApJ, 727, 1
Davis, M., Guhathakurta, P., Konidaris, N. P., et al. 2007, ApJL, 660, L1
Dickinson, M., Giavalisco, M. & GOODS Team 2003, in The Mass of Galaxies at Low and High Redshift, ed. R. Bender & A. Renzini (Berlin: Springer), 324
Donley, J. L., Koekemoer, A. M., Brusa, M., et al. 2012, ApJ, 748, 142
Draine, B. T., & Li, A. 2007, ApJ, 657, 810
Eisenhardt, P. R. M., Wu, J., Tsai, C.-W., et al. 2012, ApJ, 755, 173
Fazio, G. G., Hora, J. L., Allen, L. E., et al. 2004, ApJS, 154, 10
Fontana, A., Dunlop, J. S., Paris, D., et al. 2014, A&A, 570, A11
Gardner, J. P., Cowie, L. L., & Wainscoat, R. J. 1993, ApJL, 415, L9
Geach, J. E., Dunlop, J. S., Halpern, M., et al. 2017, MNRAS, 465, 1789
Genzel, R., Lutz, D., Sturm, E., et al. 1998, ApJ, 498, 579
Giavalisco, M., Ferguson, H. C., Koekemoer, A. M., et al. 2004, ApJL, 600, L93
Gioia, I. M., Henry, J. P., Mullis, C. R., et al. 2003, ApJS, 149, 29
Harwit, M., Munutt, D. P., Shivanandan, K., & Zajac, B. J. 1966, AJ, 71, 1026
Hatsukade, B., Kohno, K., Aretxaga, I., et al. 2011, MNRAS, 411, 102
Hemmati, S., Yan, L., Diaz-Santos, T., et al. 2017, ApJ, 834, 36
Jarrett, T. H., Cohen, M., Masci, F., et al. 2011, ApJ, 735, 112
Jeon, Y., Im, M., Ibrahimov, M., et al. 2010, ApJS, 190, 166
Jeon, Y., Im, M., Kang, E., Lee, H. M., & Matsuhara, H. 2014, ApJS, 214, 20
Jones, L. R., Fong, R., Shanks, T., Ellis, R. S., & Peterson, B. A. 1991, MNRAS, 249, 481
Kessler, M. F., Steinz, J. A., Anderegg, M. E., et al. 1996, A&A, 315, L27
Kim, S. J., Lee, H. M., Matsuhara, H., et al. 2012, A&A, 548, A29
Kollgaard, R. I., Brinkmann, W., Chester, M. M., et al. 1994, ApJS, 93, 145
Krumpe, M., Miyaji, T., Brunner, H., et al. 2015, MNRAS, 446, 911
Lacy, M., Storrie-Lombardi, L. J., Sajina, A., et al. 2004, ApJS, 154, 166
Lacy, M., Wilson, G., Masci, F., et al. 2005, ApJS, 161, 41
Lee, H. M., Im, M., Wada, T., et al. 2007, PASJ, 59, S529
Lee, H. M., Kim, S. J., Im, M., et al. 2009, PASJ, 61, 375
Le Floc'h, E., Papovich, C., Dole, H., et al. 2005, ApJ, 632, 169
Lejeune, T., Cuisinier, F., & Buser, R. 1997, A&AS, 125, 229
Lejeune, T., Cuisinier, F., & Buser, R. 1998, A&AS, 130, 65
Lonsdale, C. J., Smith, H. E., Rowan-Robinson, M., et al. 2003, PASP, 115, 897
Magnelli, B., Elbaz, D., Chary, R. R., et al. 2011, A&A, 528, A35
Makovoz, D., Roby, T., Khan, I., & Booth, H. 2006, Proc. SPIE, 6274, 62740C
Matsuhara, H., Wada, T., Matsuura, S., et al. 2006, PASJ, 58, 673
Matsumoto, T., Matsuura, S., Murakami, H., et al. 2005, ApJ, 626, 31
Matsuura, S., Arai, T., Bock, J. J., et al. 2017, ApJ, 839, 7
Mauduit, J.-C., Lacy, M., Farrah, D., et al. 2012, PASP, 124, 714
Murakami, H., Baba, H., Barthel, P., et al. 2007, PASJ, 59, S369
Murata, K., Matsuhara, H., Wada, T., et al. 2013, A&A, 559, A132
Neugebauer, G., Habing, H. J., van Duinen, R., et al. 1984, ApJL, 278, L1
Neugebauer, G., & Leighton, R. B. 1969, Two-micron Sky Survey. A Preliminary Catalogue (Washington, DC: NASA)
Oke, J. B., & Gunn, J. E. 1983, ApJ, 266, 713
Papovich, C., Moustakas, L. A., Dickinson, M., et al. 2006, ApJ, 640, 92
Pearson, C., Cheale, R., Serjeant, S., et al. 2017, PKAS, 32, 219
Pérez-González, P. G., Rieke, G. H., Egami, E., et al. 2005, ApJ, 630, 82
Pilbratt, G. L., Riedinger, J. R., Passvogel, T., et al. 2010, A&A, 518, L1
Pozzetti, L., Madau, P., Zamorani, G., Ferguson, H. C., & Bruzual, A. G. 1998, MNRAS, 298, 1133
Sanders, D. B., Salvato, M., Aussel, H., et al. 2007, ApJS, 172, 86
Saunders, W., Rowan-Robinson, M., Lawrence, A., et al. 1990, MNRAS, 242, 318
Schlegel, D. J., Finkbeiner, D. P., & Davis, M. 1998, ApJ, 500, 525
Serjeant, S., Buat, V., Burgarella, D., et al. 2012, arXiv:1209.3790
Soifer, B. T., Rowan-Robinson, M., Houck, J. R., et al. 1984, ApJL, 278, L71
Stern, D., Eisenhardt, P., Gorjian, V., et al. 2005, ApJ, 631, 163
Valiante, E., Smith, M. W. L., Eales, S., et al. 2016, MNRAS, 462, 3146
Werner, M. W., Roellig, T. L., Low, F. J., et al. 2004, ApJS, 154, 1
Westera, P., Lejeune, T., Buser, R., Cuisinier, F., & Bruzual, G. 2002, A&A, 381, 524
Wright, E. L., Eisenhardt, P. R. M., Mainzer, A. K., et al. 2010, AJ, 140, 1868
Wu, J., Tsai, C.-W., Sayers, J., et al. 2012, ApJ, 756, 96
Yasuda, N., Fukugita, M., Narayanan, V. K., et al. 2001, AJ, 122, 1104
Zacharias, N., Finch, C. T., Girard, T. M., et al. 2013, AJ, 145, 44
Zemcov, M., Smidt, J., Arai, T., et al. 2014, Sci, 346, 732